



HAL
open science

Tone generation in impinging jets with laminar and highly-disturbed nozzle-exit boundary layers

Mathieu Varé, Christophe Bogey

► **To cite this version:**

Mathieu Varé, Christophe Bogey. Tone generation in impinging jets with laminar and highly-disturbed nozzle-exit boundary layers. 29th AIAA/CEAS Aeroacoustics Conference, Jun 2023, San Diego, United States. pp.3745, 10.2514/6.2023-3745 . hal-04122925

HAL Id: hal-04122925

<https://hal.science/hal-04122925>

Submitted on 8 Jun 2023

HAL is a multi-disciplinary open access archive for the deposit and dissemination of scientific research documents, whether they are published or not. The documents may come from teaching and research institutions in France or abroad, or from public or private research centers.

L'archive ouverte pluridisciplinaire **HAL**, est destinée au dépôt et à la diffusion de documents scientifiques de niveau recherche, publiés ou non, émanant des établissements d'enseignement et de recherche français ou étrangers, des laboratoires publics ou privés.

Tone generation in impinging jets with laminar and highly-disturbed nozzle-exit boundary layers

Mathieu Varé* and Christophe Bogey†

*Univ Lyon, École Centrale de Lyon, INSA Lyon, Université Claude Bernard Lyon I, CNRS
Laboratoire de Mécanique des Fluides et d'Acoustique, UMR 5509
F-69134 Ecully, France*

The tone generation in jets with laminar and highly-disturbed nozzle-exit boundary layers impinging on a plate is investigated. Seven initially laminar jets and seven jets with a nozzle-exit turbulent intensity of 9% are considered. The jets all impinge on a plate located at a distance of 8 nozzle radii from the nozzle and have Mach numbers M ranging from 0.6 to 1.3. For $M \leq 0.8$ for the laminar jets and for $M = 0.6$ for the highly-disturbed jets, the sound radiation is broadband. For higher Mach numbers, tones emerge by more than 10 dB in the near-nozzle pressure spectra for both exit boundary-layer states. The tones are produced by feedback loops establishing between the nozzle and the plate, involving downstream-travelling Kelvin-Helmholtz instability waves and upstream-travelling guided jet waves. The tone frequencies do not depend on the state of the boundary layer. They are organized into stages as the Mach number increases and they fall in the frequency bands of the guided jet waves closing the feedback loop. Moreover, for both initially laminar and highly-disturbed jets, the dominant tone is related to an axisymmetric oscillation mode, except for $M = 1.1$. In the latter case, tones of similar amplitudes are linked to the axisymmetric and the first helical modes. Therefore, the azimuthal structure of the jet is not significantly affected by the nozzle-exit turbulent intensity. This is not the case for the levels and prominence of the tones, which are lower for the initially laminar jets than for the other ones, suggesting a weaker resonance in the former case. This weaker resonance appears to be due to a lower amplification of the shear-layer instability waves between the nozzle and the plate at the tone frequencies.

I. Introduction

Intense acoustic tones are known to be produced by high-speed jets impinging on a flat plate. They have been first noticed for high subsonic jets in many experimental works, such as those of Marsh [1], Preisser [2], Neuwerth [3] or Ho & Nosseir [4, 5]. They were later found to be emitted by supersonic jets, as shown in the experiments of Norum [6], Krothapalli *et al.* [7] and Henderson *et al.* [8–10] and in the simulations of Dauptain *et al.* [11] and Gojon *et al.* [12–14], for example. Similar tones are also observed for jets impinging on edges [15] and perforated or inclined plates [16–19]. The tone frequencies exhibit a staging behaviour with the nozzle-to-plate distance, which has led Powell [15] to attribute their generation to aeroacoustic feedback loops establishing between the nozzle and the plate. The downstream component of the loops consists of the flow disturbances convected in the jet mixing layers, related to Kelvin-Helmholtz instability waves. The upstream component is formed by upstream-propagating guided jet waves [20], defined by specific dispersion relations and organized into azimuthal and radial modes. The latter waves also play a role in other resonance phenomena, such as in jet-flap interactions [21, 22] and screech noise generation [23–26]. They are also responsible for the production of acoustic tones in the near pressure fields of free jets [27–30]. Furthermore, the properties of the feedback mechanisms in impinging jets are affected by the jet Mach number. Ho & Nosseir [4, 5] observed experimentally that no feedback loop establishes for Mach numbers lower than 0.7. In other experiments [3, 20, 31], only an axisymmetric feedback mode is found for subsonic jets whereas both axisymmetric and helical feedback modes can be noticed for supersonic jets. Moreover, the influence of the Mach number on the feedback frequencies has been investigated experimentally by Jaunet *et al.* [32] and numerically by Varé & Bogey [33] for jets at Mach numbers varying between 0.6 and 1.3. In both studies, a staging behaviour of the tone frequencies with the Mach number is remarked, which is a feature of resonance phenomena. The tone frequencies are located in the allowable frequency bands of the upstream-propagating guided jet waves, as expected given that the latter

*Postdoctoral fellow, mathieu.vare@ec-lyon.fr

†CNRS Research Scientist, AIAA Senior Member & Associate Fellow, christophe.bogey@ec-lyon.fr

waves close the feedback loop. However, for Mach numbers lower than 0.9, the tone frequencies in the simulations are significantly higher than those in the experiments. This discrepancy was attributed to different nozzle-exit conditions between the experiments and the simulations. Among the nozzle-exit conditions, the state of the boundary layers at the nozzle exit may be of great importance. Indeed, for free jets, the laminar or turbulent state of the nozzle-exit boundary layers strongly affects the flow development and the noise generation mechanisms, as documented in many works [34–37]. For initially laminar jets, roll-ups of the shear layer and pairings of vortical structures occur, which is not the case for initially turbulent jets. Strong pressure waves are radiated by these vortex pairings, leading to higher noise levels compared with those for initially turbulent jets.

Despite the preceding studies, the influence of the initial state of the boundary layer on resonance mechanisms in impinging jets is still unclear. The effects of this state on the establishment of feedback loops between the nozzle and the plate and on the Mach number variations of the tone properties, namely their frequencies, amplitudes and azimuthal structures, need to be highlighted.

In the present work, the tone generation in impinging jets is investigated by performing the large-eddy simulations (LES) of fourteen impinging jets at Mach numbers varying between 0.6 and 1.3, with laminar or highly-disturbed nozzle-exit boundary layers. The jets are at a Reynolds number of 10^5 and they impinge on a plate located at 8 nozzle radii from the nozzle. Half of the jets have initially laminar boundary layers and the other half have highly-disturbed nozzle-exit boundary layers, with a peak turbulent intensity of 9%. The first objective of this work is to study the effects of the state of the nozzle-exit boundary layers on the establishment of feedback loops between the nozzle and the plate. For that purpose, the flow and sound fields are described. The near-nozzle pressure spectra are examined to highlight the emergence of tones. The contributions of the first two azimuthal modes to the pressure fields are investigated to determine the azimuthal structure of the jets at the tone frequencies. The Mach number variations of the frequencies, amplitudes, widths and prominence of the tones are detailed. The results for the initially laminar jets are systematically compared with those for the initially highly-disturbed jets to discuss the effects of the nozzle-exit boundary-layer states on the tones. Another aim of the work is to study the influence of the initial flow conditions on the flow development of the jets by examining velocity spectra in the shear layer. The last objective of this paper is to discuss possible variations of the tone amplitudes with the initial state of the jet mixing layer. To this end, the power gains of the Kelvin-Helmholtz instability waves between the nozzle and the plate are computed at the tone frequencies.

This paper is organized as follows. The jet parameters and the numerical methods used in the LES are documented in section II. The results of the simulations are presented in section III. Vorticity and pressure snapshots, mean and turbulent flow fields and pressure spectra are first described. The Mach number variations of the frequencies, amplitudes, widths and prominences of the tones are shown for both initially laminar and highly-disturbed jets. The velocity spectra in the shear layer are presented. The amplification of the shear-layer instability waves between the nozzle and the plate is evaluated at the tone frequencies using linear stability analysis. Finally, concluding remarks are given in section IV.

II. Parameters

A. Jet parameters

The jets computed in this work have a Reynolds number $Re_D = u_j D / \nu$ of 10^5 , where u_j is the jet velocity, D the nozzle diameter and ν the air kinematic viscosity. They originate at $z = 0$ from a cylindrical nozzle of radius r_0 and length $2r_0$, and are at ambient pressure and temperature $p_0 = 10^5$ Pa and $T_0 = 293$ K. They impinge on a plate located at $L = 8r_0$ downstream of the nozzle exit, as in the experiments of Jaunet *et al.* [32]. At the nozzle inlet, a Blasius laminar boundary-layer profile with a thickness of $0.15r_0$ is imposed for the velocity. In the pipe, the boundary layers are tripped or not, yielding highly-disturbed or fully laminar nozzle-exit boundary layers. Seven jets are tripped by adding vortical disturbances uncorrelated in the azimuthal direction in the boundary layer at $z = -r_0$ to create velocity fluctuations at the nozzle exit, using a procedure described in Bogey *et al.* [38]. The seven other jets are untripped. For both exit boundary-layer states, the jets have Mach numbers of $M = 0.6, 0.75, 0.8, 0.9, 1, 1.1$ and 1.3 . The profiles of root-mean-square (r.m.s.) axial velocity fluctuations at the nozzle exit are presented in figure 1. In all cases, the turbulent intensity reaches a peak value around $r = 0.98r_0$. For the untripped jets in figure 1(a), this value increases with the Mach number, from 0.25 % at $M = 0.6$ up to 1.45 % at $M = 1.3$, whereas for the tripped jets in figure 1(b), it is equal to 9 % for all Mach numbers, as expected. The nozzle-exit velocity fluctuations for the initially laminar jets are not zero as the mixing layers are excited by upstream-propagating pressure waves.

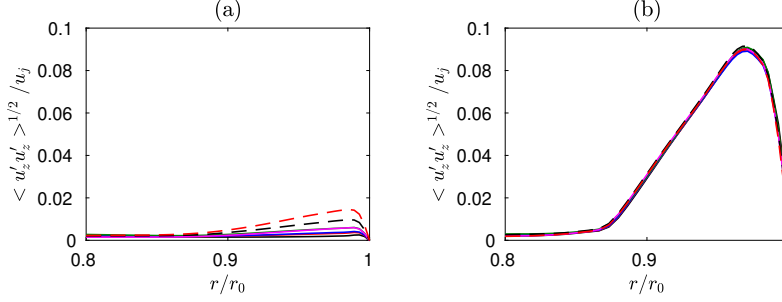


Fig. 1 Nozzle-exit profiles of r.m.s. values of axial velocity for the jets with (a) untripped and (b) tripped boundary layers at — $M = 0.6$, — $M = 0.75$, — $M = 0.8$, — $M = 0.9$, — $M = 1$, - - - $M = 1.1$ and - - - $M = 1.3$.

B. Numerical parameters

In the simulations, the unsteady compressible Navier-Stokes equations are solved in cylindrical coordinates (r, θ, z) using an OpenMP based in-house solver. A second-order, six-stage Runge-Kutta algorithm [39] is employed for time-integration and the spatial derivatives are computed with eleven-point low-dispersion finite-difference schemes [40]. At the end of each time step, a selective filtering is applied to remove grid-to-grid oscillations [39]. This filter also acts as a subgrid-scale model ensuring the relaxation of turbulent kinetic energy near the grid cut-off frequency [41]. No-slip and adiabatic wall conditions are imposed to the plate and nozzle walls. In order to handle possible shocks created by the jet impingement in the jet potential core, a damping procedure using a dilatation-based shock detector and a second-order filter is used to remove Gibbs oscillations in the vicinity of shocks for $z \geq 3r_0$ [42]. The radiation boundary conditions of Tam & Dong [43] are implemented at the radial and lateral boundaries of the computational domain. They are associated with sponge zones combining grid stretching and Laplacian filtering to prevent significant spurious reflections [44]. The method of Mohseni & Colonius [45] is applied to treat the singularity on the jet axis. The closest point to the axis is located at $r = \Delta r/2$, where Δr is the radial mesh size near the jet axis. The azimuthal derivatives near the jet axis are evaluated with fewer points than permitted by the grid to increase the time step of the simulations [46]. More precisely, the effective azimuthal resolution near the origin of the polar coordinates is reduced down to $2\pi/16$.

C. Computational parameters

The same radial and axial mesh grids, presented in Varé & Bogey [33], are used for all simulations. The numbers of points in the radial and axial directions are equal to 559 and 1124. In the azimuthal direction, there are 1024 points for the tripped jets and 256 points for the untripped jets, which yields a total number of 640 and 160 million points, respectively. The grid extends out to $r = 15r_0$ in the radial direction and down to $z = 8r_0$ in the axial direction. The radial mesh spacing is equal to $\Delta r = 0.014r_0$ on the jet axis and decreases down to $\Delta r = 0.0036r_0$ at $r = r_0$ in the shear layer. It then increases up to a maximum value of $\Delta r = 0.075r_0$ for $r > 6.2r_0$, which yields Strouhal numbers $St = fD/u_j$ varying from 4.1 at $M = 1.3$ up to 8.9 at $M = 0.6$ for an acoustic wave with five points per wavelength. The axial mesh spacing Δz is minimum and equal to $\Delta z = 0.0072r_0$ at the nozzle exit, and maximum and equal to $\Delta z = 0.012r_0$ between $z = 2r_0$ and $z = 6r_0$. Farther downstream, the axial mesh spacing decreases down to $\Delta z = 0.0072r_0$ near the plate at $z = 8r_0$. The extremum values of the mesh spacings and the stretching rates are the same as in the study of Bogey [47], where a grid convergency study was performed for a free jet with the same ejection conditions as the impinging tripped jet at $M = 0.9$ of the present work. The results presented are obtained after simulation times of $500r_0/u_j$ for the tripped jet at $M = 1.3$ and $1000r_0/u_j$ for the other jets. During the simulations, density, velocities and pressure along the jet centerline at $r = 0$, along the nozzle-lip line at $r = r_0$, on the surfaces at $r = 15r_0$, $z = -2r_0$, $z = 0$ and on the plate at $z = L$ are recorded at a sampling frequency enabling spectra to be computed up to $St = 12$. Density, velocity components and pressure are also saved at the azimuthal angles $\theta = 0, 90, 180$ and 270 degrees at a halved frequency. The azimuthal Fourier coefficients of the density, pressure and velocity fields are also computed up to the mode $n_\theta = 4$ for $0 \leq r \leq 15r_0$ and $0 \leq z \leq 8r_0$. The spectra are estimated from these recordings and they are averaged in the azimuthal direction when possible.

III. Results

A. Snapshots of the flow and acoustic fields

Snapshots of the vorticity norm and of the pressure fluctuations are presented in figure 2 for the untripped and tripped jets at Mach numbers of 0.6, 0.8, 1.1 and 1.3 on top and bottom, respectively. The results for the jets at $M = 0.75$ resemble those for the jets at $M = 0.8$ and the results for $M = 0.9$ and 1 look like those for $M = 1.3$. Therefore, for brevity, they are not shown here. In the vorticity fields, for the untripped jets in figure 2(a-d), roll-ups of the shear layer and pairings of large coherent structures are observed from the nozzle exit down to $z = 4r_0$ whereas for the tripped jets in figure 2(e-h), fine-scale turbulent structures are found near the nozzle exit, indicating highly-disturbed mixing layers. For the two exit boundary-layer states, the shear layers spread as the axial distance increases and they impinge on the plate, which creates a wall jet.

In the pressure fields, for the tripped jets for $M \geq 0.8$ in figure 2(f,g,h), strong low-frequency pressure waves originating from the impingement area dominate in the sound field. Their wavefronts are clearly periodically spaced, indicating a tonal radiation. They also propagate in the upstream direction inside the jet column. For the untripped jets at $M = 1.1$ and 1.3 in figures 2(c,d), pressure waves similar to those for the corresponding tripped jets are observed. However, their amplitudes are lower than for the tripped jets, suggesting a weaker resonance. For the untripped jets at $M = 0.6$ and 0.8 and the tripped jet at $M = 0.6$ in figures 2(a,b,e), high-frequency pressure waves are seen to be produced near the plate and the wall jet and to propagate in the upstream direction. The sound radiation does not appear to be tonal.

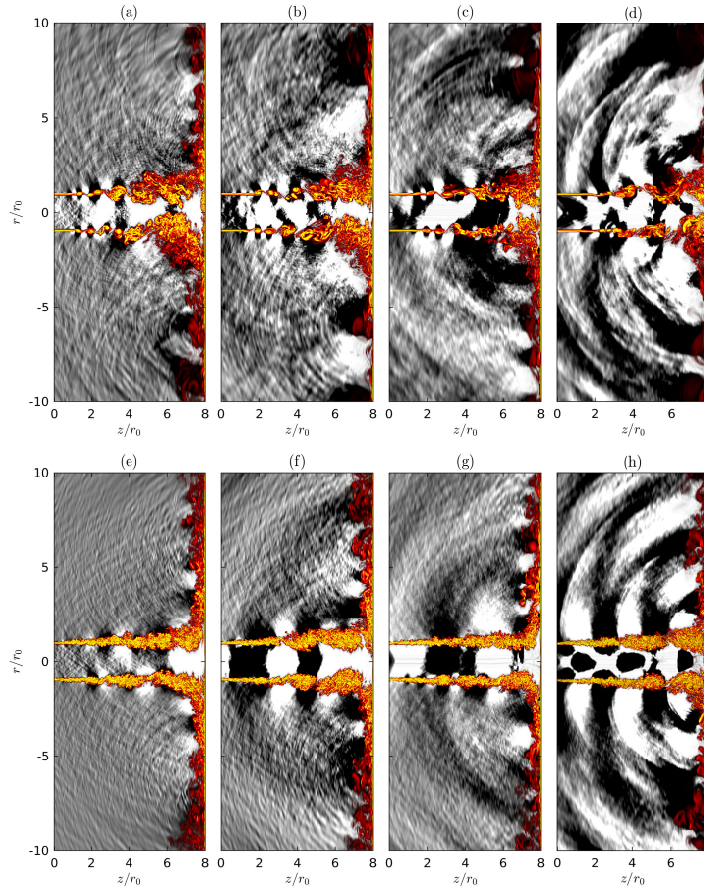


Fig. 2 Snapshots in the (z, r) plane of vorticity norm in the flow and of pressure fluctuations outside for (top) untripped and (bottom) tripped jets at (a,e) $M = 0.6$, (b,f) $M = 0.8$, (c,g) $M = 1.1$ and (d,h) $M = 1.3$. The color scales range from 0 to $15u_j/r_0$ for vorticity, from black to yellow, and between (a,b,e,f) $\pm 0.005p_0$ and (c,d,g,h) $\pm 0.01p_0$ for pressure, from black to white.

B. Mean flow fields

The centerline mean axial velocity, the shear-layer momentum thickness and the axial turbulent intensity at $r = r_0$ obtained between the nozzle and the plate are shown in figure 3. In figure 3(a,d), for all jets, the centerline mean velocity is close to the exit velocity down to $z = 6.5r_0$, and falls down to zero on the plate at $z = 8r_0$. For the initially laminar jets in figure 3(a), small velocity oscillations are noticed between $z = 0$ and $z = 6r_0$ for $M \geq 1.1$, due to the presence of weak shock cells. For the initially disturbed jets in figure 2(d), velocity oscillations are observed for $M \geq 0.9$. Their amplitude is especially high for $z \geq 4r_0$, suggesting that they are related to compression cells created by the jet impingement on the plate. They are stronger than for the untripped jets, indicating that the mean flow fields of the tripped jets are more affected by the jet impingement on the plate than those of the untripped jets.

In figures 3(b,e), for a given exit boundary-layer state, the shear-layer thicknesses are similar for all Mach numbers. However, they are significantly different in the tripped and the untripped cases. The mixing layer starts to spread at $z = 2r_0$ for the untripped jets in figure 3(b) and at $z = 0$ for the tripped jets in figure 3(e). Then, the shear-layer thickness grows almost linearly down to $z \approx 6.5r_0$. The shear-layer growth rate is lower for the tripped jets than for the untripped ones, which is consistent with the results obtained for free jets [36]. Near the plate, in all cases, the shear-layer thickness increases due to the formation of a wall jet.

The variations of the axial turbulent intensity in figure 3(c,f) are similar for all Mach numbers, but they depend on the nozzle-exit conditions. For the untripped jets in figure 3(c), the amplitudes of the axial velocity fluctuations are very low down to $z = r_0$ and then quickly increase up to about 20 % of the jet exit velocity at $z = 3r_0$. This strong increase is related to the vortex pairings occurring in the shear layer. Farther downstream, the turbulent levels do not vary much down to $z = 7r_0$ and finally decrease down to zero on the plate. For the tripped jets in figure 3(f), the axial turbulent intensities strongly rise just downstream of the nozzle exit down to $z = 2r_0$. Then they remain almost constant down to $z = 7r_0$, with values between 13 % for $M = 0.9$ and 16 % for $M = 0.6$, and fall down to zero on the plate. The peak values of the axial turbulent intensity along the nozzle-lip line are significantly lower for the tripped jets than for the untripped ones.

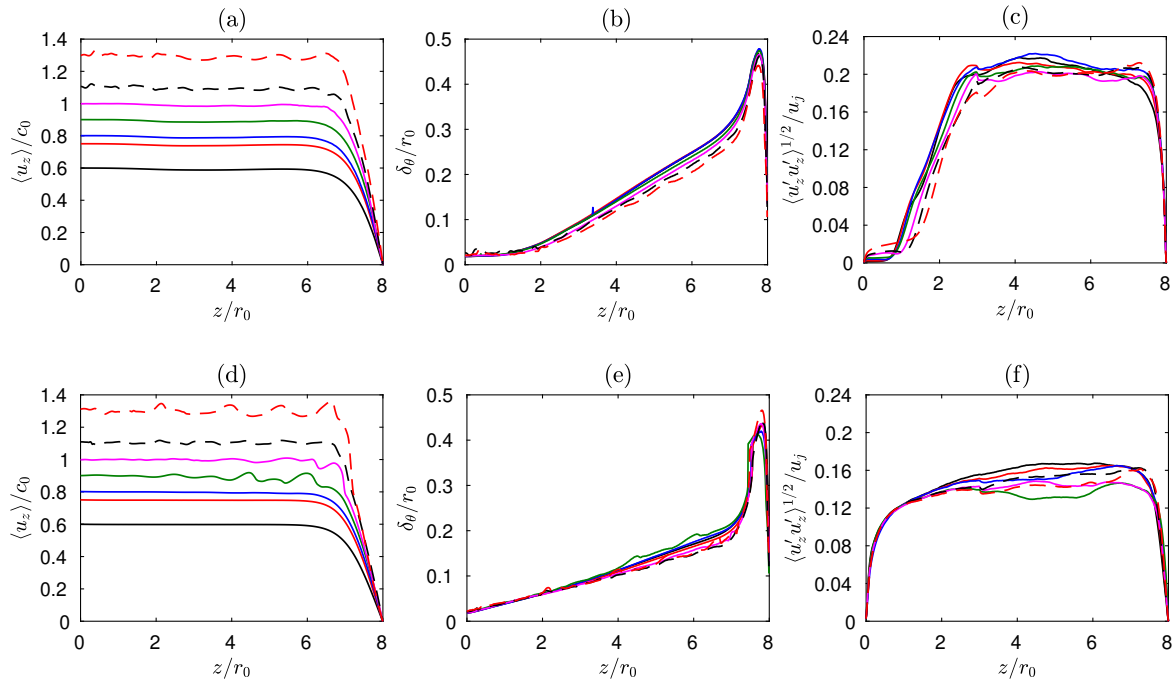


Fig. 3 Variations of (a,d) the centerline mean axial velocity $\langle u_z \rangle / c_0$, (b,e) the shear-layer momentum thickness δ_θ / r_0 and (c,f) the axial turbulent intensity $\langle u'_z u'_z \rangle^{1/2} / u_j$ at $r = r_0$ for (top) untripped jets and (bottom) tripped jets; — $M = 0.6$, — $M = 0.75$, — $M = 0.8$, — $M = 0.9$, — $M = 1$, - - - $M = 1.1$ and - - - $M = 1.3$.

C. Near-nozzle pressure spectra

The pressure spectra obtained at $z = 0$ and $r = 1.5r_0$ near the nozzle are displayed in figure 4 for the jets at $M = 0.6, 0.8, 1.1$ and 1.3 as a function of the Strouhal number. The spectra for the jets at $M = 0.75$ follow the same tendencies as those for $M = 0.8$ and the spectra for $M = 0.9$ and 1 are similar to those for $M = 1.3$. Hence, they are not shown here. In all cases, the broadband levels are approximately 5 dB higher for the untripped jets than for the tripped ones. For $M = 0.6$, in figure 4(a), no tones are clearly seen in the spectra, indicating the absence of marked resonance phenomena. For $M = 0.8$ in figure 4(b), a tone appears 15 dB higher than the broadband levels at $St = 0.51$ for the tripped jet but not for the untripped one. For higher Mach numbers in figures 4(c,d), peaks emerging by more than 10 dB are found for both tripped and untripped jets. Their frequencies are similar in the two cases. They are equal to $St = 0.29, 0.46$ and 0.66 for $M = 1.1$ in figure 5(c) and to $St = 0.35$ and 0.51 for $M = 1.3$ in figure 5(d). Regarding the tone amplitudes, they are higher for the initially highly-disturbed jets than for the initially laminar jets. They are examined in more detail later in section III.D.

In all cases, the tones are produced by aeroacoustic feedback loops establishing between the nozzle and the plate. To predict the feedback frequencies, Ho & Nosseir [4] considered that the feedback period is the sum of two characteristic times, namely the time of convection of the flow structures from the nozzle exit down to the plate and the time of propagation of the upstream-propagating acoustic waves. The feedback frequencies can thus be estimated by

$$f = \frac{N\langle u_c \rangle}{L(1 + M_c)} \quad (1)$$

where $\langle u_c \rangle$ is the mean convection velocity between the nozzle and the plate, $M_c = \langle u_c \rangle / c_0$ is the convection Mach number and N is an integer representing the order of the feedback mode. The integer N corresponds to the number of coherent structures between the nozzle and the plate. Each tone frequency can thus be related to an integer N , as will be discussed in section III.D.

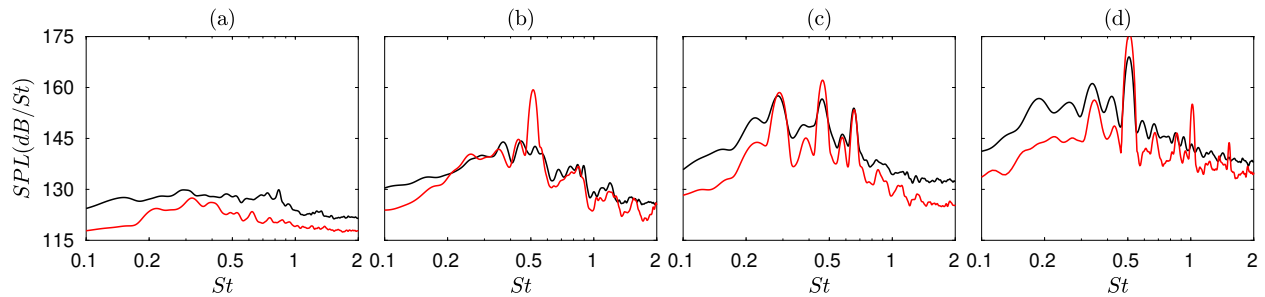


Fig. 4 Sound pressure levels (SPL) at $z = 0$ and $r = 1.5r_0$ for (a) $M = 0.6$, (b) $M = 0.8$, (c) $M = 1.1$ and (d) $M = 1.3$; — untripped and — tripped jets.

The contributions of the first two azimuthal modes to the pressure spectra at $z = 0$ and $r = 1.5r_0$ are presented in figure 5 for $M = 0.6, 0.8, 1.1$ and 1.3 , as previously. For each Mach number, the dominant oscillation modes are the same. For $M = 0.6$ in figures 5(a,e), the contributions of the mode $n_\theta = 0$ are predominant for Strouhal numbers lower than 0.9 . For $St > 0.9$, the levels for $n_\theta = 0$ decrease more rapidly than for the full signals, by 20 dB for the untripped jet and by 10 dB for the tripped jet. The decrease is sharper in the first case because of the presence of a peak at $St = 0.83$. For higher frequencies, the contributions of the mode $n_\theta = 1$ to the pressure field are significant for both initial flow conditions. For $M = 0.8$ in figures 5(b,f), the maximum levels are found for the mode $n_\theta = 0$. In the untripped case in figure 5(b), they are reached in a hump between $St = 0.2$ and 0.6 containing three weakly emerging peaks at $St = 0.37, 0.45$ and 0.51 , whereas for the tripped case in figure 5(f), they are related to the presence of an intense tone at $St = 0.51$. In both cases, secondary peaks are visible at $St = 1.2$ for $n_\theta = 0$ and at $St = 0.9$ and 1.5 for $n_\theta = 1$. For $M = 1.1$ in figures 5(c,g), the tones at $St = 0.29$ and 0.66 are linked to the axisymmetric mode, whereas the tone at $St = 0.46$ is related to the first helical mode. Interestingly, the peaks at $St = 0.29$ and 0.46 have similar amplitude for the untripped jet, but the second peak is roughly 4 dB higher than the first one for the tripped jet. Finally, for $M = 1.3$ in figures 5(d,h), the dominant peak at $St = 0.51$ is associated with the mode $n_\theta = 0$ and secondary peaks are noticed at $St = 0.2$ for $n_\theta = 0$ and around $St = 0.35$ for $n_\theta = 1$. The first two harmonics of the tone at $St = 0.51$ for $n_\theta = 0$ and the first harmonic of the peak at $St = 0.35$ for $n_\theta = 1$ emerge by more than 10 dB above the broadband noise for the initially highly-disturbed jet, which is not the case for the other jet.

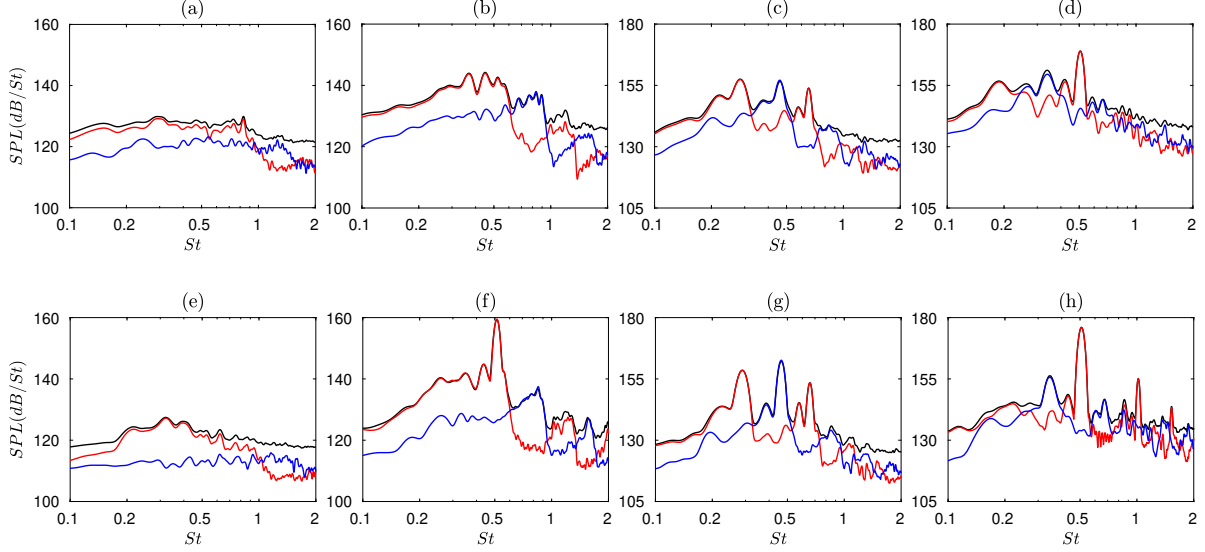


Fig. 5 Sound pressure levels (SPL) at $z = 0$ and $r = 1.5r_0$ for (top) untripped and (bottom) tripped jets at (a,e) $M = 0.6$, (b,f) $M = 0.8$, (c,g) $M = 1.1$ and (d,h) $M = 1.3$; — full signal, — $n_\theta = 0$ and — $n_\theta = 1$.

D. Mach number variations of the near-nozzle tone properties

The peak Strouhal numbers in the near-nozzle pressure spectra for the first two azimuthal modes are plotted in figure 6 as a function of the Mach number. For $n_\theta = 0$, in figure 6(a), for $M = 0.6$, the peak frequency is about three times higher in the untripped case than in the tripped case. For $M = 0.75$ and 0.8 , inversely, the peak frequencies are significantly lower in the first case. For higher Mach numbers, they are similar for the two initial flow conditions. For $n_\theta = 1$ in figure 6(b), the peak frequencies are also the same for the two flow states at all Mach numbers.

In the figures, the frequency ranges of the free-stream upstream-propagating guided jet waves estimated using a vortex-sheet model are indicated. Each band is associated with a radial mode of the guided jet waves, whose order n_r increases with the frequency. For $n_\theta = 0$, the dominant tones lie in the band of the first radial mode for $M \leq 1.1$ and of the second radial mode for $M = 1.3$. For $n_\theta = 1$, they are all located in the band of the first radial mode. In particular, for $n_\theta = 0$ and $n_r = 1$ in figure 6(a), the dominant tones are close to the mode cutoff frequency for the jets emitting intense tones, namely the jets at $M \geq 0.9$ and the tripped jets at $M = 0.75$ and 0.8 , which has also been observed for the near-nozzle tones of free jets [29]. In contrast, they are far from this limit for the untripped jets at $M = 0.75$ and 0.8 and the tripped jet at $M = 0.6$ generating no tones. For the untripped jet at $M = 0.6$, the peak frequency is near the upper limit of the guided jet mode, suggesting that the small peak at $St = 0.83$ in the pressure spectrum is produced by a weak resonance.

In figure 6, the frequencies predicted by equation (1) are also plotted. For both modes, the peak frequencies fall close to curves given by this model whatever the initial flow condition, for different feedback modes N . For example, for $n_\theta = 0$ for the tripped jets, the mode order is equal to $N = 3$ for $M = 0.6$, jumps to $N = 6$ for $M = 0.75$, then as the Mach number increases, it is reduced down to $N = 3$ at $M = 1.1$ and finally it increases up to $N = 6$ for $M = 1.3$. These changes in the feedback mode order can be explained by the closure of the loops by the guided jet waves. Indeed, the values of N vary so that the tone frequencies stay in the bands of the guided jet waves. Notably, for $n_\theta = 0$, the feedback mode N rises from $N = 3$ at $M = 1.1$ to $N = 6$ at $M = 1.3$ as the tonal frequency switches from the first radial mode of the guided jet waves at $M = 1.1$ to the second radial mode at $M = 1.3$ [33].

The Mach number variations of the amplitude, width and prominence of the near-nozzle tones for $n_\theta = 0$ are displayed in figure 7. In figure 7(a), the peak levels for $M = 0.6$ and $M = 1.1$ do not change much with the nozzle-exit conditions. For other jet velocities, the tone intensities are higher by 7 to 15 dB for the tripped jets than for the untripped jets. In figure 7(b), the peak widths at half maximum for $M \leq 0.8$ and $M = 1.3$ are slightly higher for the tripped cases than for the untripped cases. On the contrary, for other Mach numbers, the peaks are two to three times thinner for the tripped jets than for the untripped jets. The prominence of the peaks, estimated as the differences between the peak levels and the first minimum values reached for higher frequency [29], is plotted in figure 7(c). For the jets at $M = 0.6$,

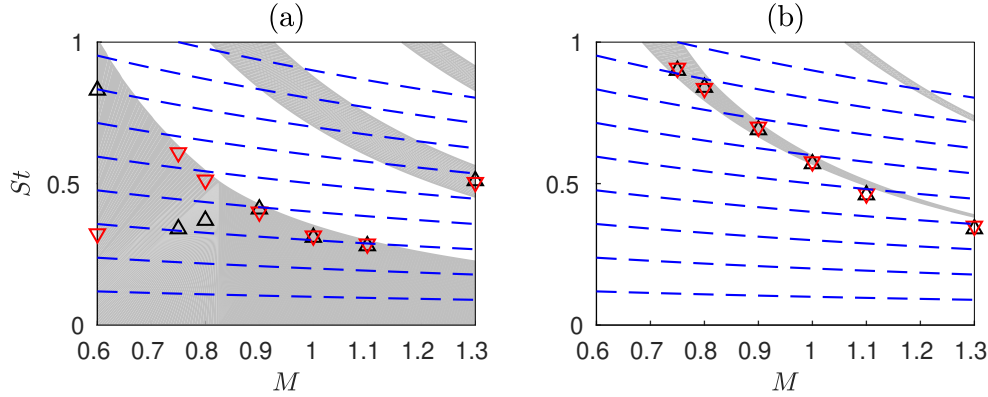


Fig. 6 Mach number variations of the peak Strouhal numbers in the near-nozzle pressure spectra for (a) $n_\theta = 0$ and (b) $n_\theta = 1$: \triangle untripped and ∇ tripped jets, (grey shading) allowable frequency bands of the free-stream upstream-propagating guided jet waves; - - - equation (1) with N varying from 1 to 9 and $\langle u_c \rangle = (2/3)u_j$.

the peak at $St = 0.83$ in the spectrum for the untripped jet emerge more strongly than the hump at $St = 0.33$ in the spectrum of the tripped jet. For higher Mach numbers, the peaks are more prominent for the highly-disturbed jets than for the initially laminar jets due to higher broadband levels in the latter case.

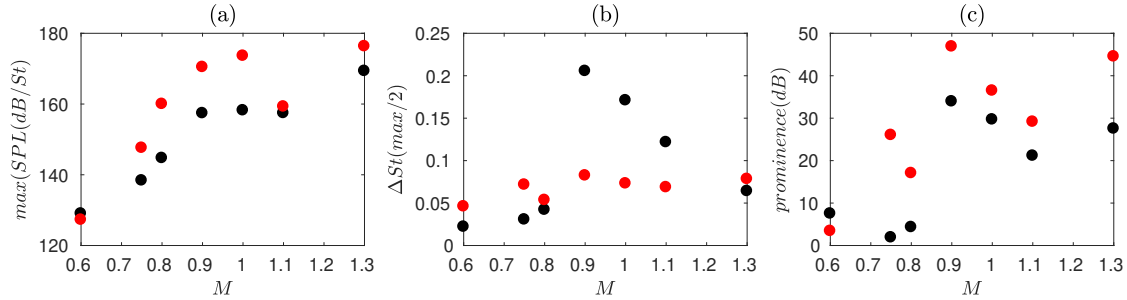


Fig. 7 Mach number variations of (a) the amplitude, (b) the width and (c) the prominence of the dominant near-nozzle tones for $n_\theta = 0$: \bullet untripped jets, \bullet tripped jets.

E. Shear-layer velocity spectra

To examine the development of the jet flow structures, the power spectral densities of the radial velocity fluctuations in the shear layer at $r = r_0$ between the nozzle exit and the plate are represented in figure 8 for the jets at $M = 0.6, 0.8, 1.1$ and 1.3 for the two exit boundary-layer states. For the untripped jets, for $M = 0.6$ and 0.8 in figures 8(a,b), two spots of strong levels are visible. The first spot is found near the nozzle at $z = 2r_0$ for Strouhal numbers between 1.5 and 2. These frequencies are close to that of $St_\theta = f\delta_\theta(z=0)/u_j = 0.016$ predicted for the most amplified Kelvin–Helmholtz instability waves at the nozzle exit using linear stability analysis [48]. The second spot lies between $z = 2r_0$ and $5r_0$ and between $St = 0.25$ and 1.2. The strongest levels in this spot are reached at frequencies close to the first subharmonic of the initial instability frequency. They result from the pairings of vortical structures in the shear layer. For $M = 0.6$, the small peak in the near-nozzle pressure spectrum at $St = 0.83$ is close to this frequency, suggesting that it can be produced by a weak feedback loop between the pressure waves generated by the vortex pairings and the Kelvin–Helmholtz instability waves, as in initially laminar free jets at similar Mach numbers [29]. For $M = 1.1$ and 1.3 in figures 8(c,d), the levels are significant in two zones at $St \approx 1.2$ and its first subharmonic, in agreement with the presence of vortex pairings in the mixing layer. However, the highest levels are located along a thin line starting at $z \approx 2r_0$ and extending down to the plate. This line is found at the Strouhal numbers of the dominant tones in the pressure spectra, highlighting a forcing of the flow structures by upstream-propagating pressure waves.

For the highly-disturbed jets, for $M = 0.6$ and $M = 0.8$ in figures 8(e,f), the power spectral densities strongly differ from those for the initially laminar jets. Only one large spot is visible near the plate for $z \geq 4r_0$ and for $St \leq 1$, farther downstream and at frequencies lower than the second spot for the untripped cases. This spot is due to the presence of a broadband hump in the velocity spectra, related to the formation of large coherent flow structures. For $M = 0.8$ in figure 8(f), two stripes of high energy are also observed at $St = 0.51$ and its first harmonic, indicating the development of flow structures at the feedback frequencies. For higher Mach numbers in figure 8(g,h), intense levels are found along lines at the frequencies of the tones in the near-nozzle pressure spectra, as for the non-disturbed jets. For $M = 1.1$, in figure 8(g), the highest levels are found at $St = 0.46$, vs $St = 0.66$ for the initially laminar jet, revealing a different excitation of the flow depending on the initial mixing-layer state. For $M = 1.3$, in figure 8(g), the components at $St = 0.51$ are dominant as for the untripped jet. High intensity is observed at the first harmonic of this frequency, which is not the case for the untripped jet. The forcing of the jet flow at the feedback frequency thus appears to be stronger for the highly-disturbed case than for the initially laminar case.

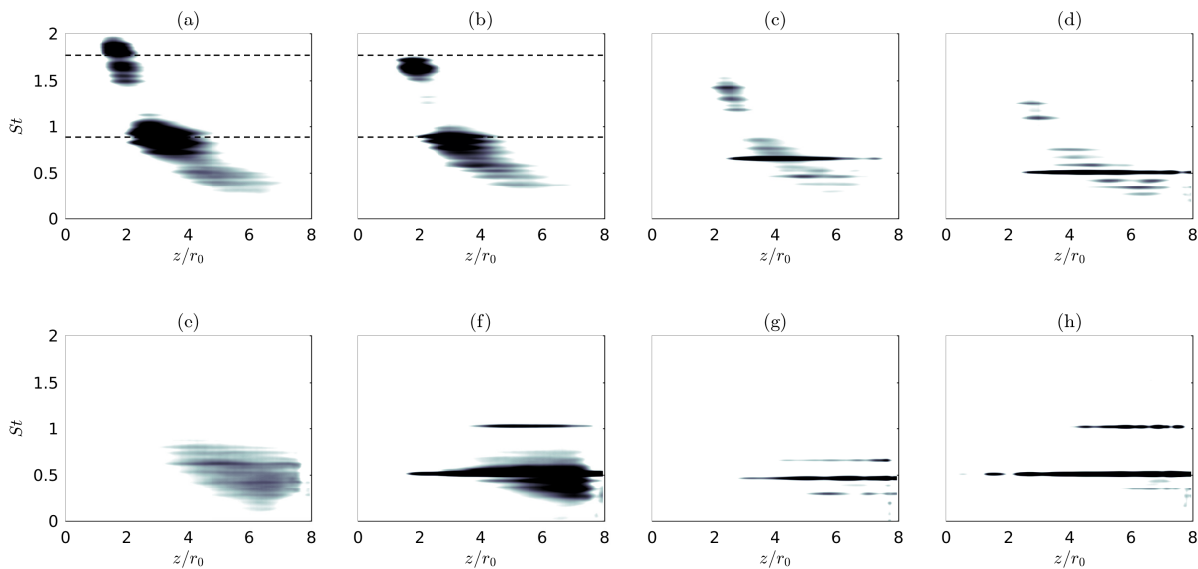


Fig. 8 Power spectral densities of the fluctuations of radial velocity normalized by the jet velocity u_j at $r = r_0$ between the nozzle and the plate for the (top) untripped and (bottom) tripped jets for (a,e) $M = 0.6$, (b,f) $M = 0.8$, (c,g) $M = 1.1$ and (d,h) $M = 1.3$, - - - $St_\theta = f\delta_\theta(z = 0)/u_j = 0.016$ and 0.08 . The color scale is 6 dB higher for the untripped jets than for the tripped ones and spreads over 3 dB, from white to black.

Spectra of the radial velocity fluctuations and the contributions of the first two modes to these spectra estimated near the nozzle and near the plate for the jets at $M = 0.6, 0.8, 1.1$ and 1.3 are now considered. The spectra near the nozzle, at $r = r_0$ and $z = 0.4r_0$, are plotted in figure 9 as a function of the Strouhal number. For the untripped jets in figures 9(a-d), for the full signals and for both $n_\theta = 0$ and 1 , a broadband hump is visible near the frequency of the most amplified instability waves at the nozzle exit, indicating the growth of the latter waves. For $M \geq 0.8$ in figures 9(b-d), in addition to this hump, low-frequency tones can be seen in the spectra. For $M = 0.8$ in figure 9(b), two tones are found around $St = 0.55$ for $n_\theta = 0$ and $St = 0.9$ for $n_\theta = 1$, suggesting a forcing of the flow by pressure waves despite the absence of tones at these frequencies in the pressure spectra of figure 5(b). For $M = 1.1$ and 1.3 in figures 9(c,d), the tones are at the same frequencies and for the same azimuthal modes as the tones in the near-nozzle pressure spectra.

For the highly-disturbed jets in figure 9(e-h), the levels of the components in the full signals are stronger than those for the initially laminar jets, due to higher nozzle-exit velocity fluctuations, as expected. As for the contributions of the first two azimuthal modes, they display a wide hump centered around the frequency of the most unstable Kelvin-Helmholtz waves, as for the untripped jets. For $M \geq 0.8$ in figures 9(f-h), for $n_\theta = 0$ and $n_\theta = 1$, intense tones are also found at frequencies similar to the tone frequencies for the initially laminar jets. They emerge more sharply than for the untripped cases, suggesting a stronger excitation of the flow by the upstream-propagating pressure waves in this case. Moreover, for $M = 1.1$ in figure 9(g), among the three tones at $St = 0.29, 0.46$ and 0.66 , the tone at $St = 0.46$ for $n_\theta = 1$ is clearly higher than the two other tones for $n_\theta = 0$, whereas the amplitudes of the three tones are similar for the untripped jet in

figure 9(c). This result suggests that the receptivity of the jet at the nozzle exit to axisymmetric and helical disturbances can be affected by the initial flow conditions.

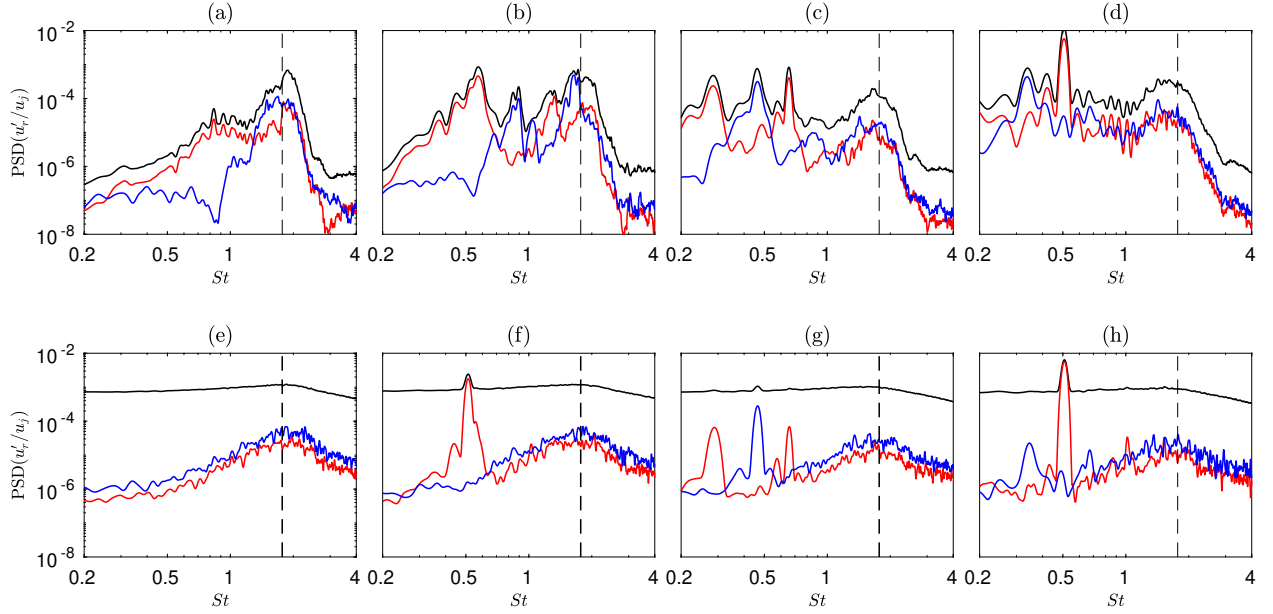


Fig. 9 Power spectral densities of the fluctuations of radial velocity at $r = r_0$ and $z = 0.4r_0$ for the (top) untripped and (bottom) tripped jets for (a,e) $M = 0.6$, (b,f) $M = 0.8$, (c,g) $M = 1.1$ and (d,h) $M = 1.3$, — full signal, — $n_\theta = 0$ and — $n_\theta = 1$, - - - $St_\theta = f\delta_\theta(z = 0)/u_j = 0.016$.

The spectra of the radial velocity fluctuations obtained near the plate at $r = r_0$ and $z = 7r_0$ are presented in figure 10. For all jets, be they tripped or not, a low-frequency hump is seen around $St = 0.5$ due to the formation of large coherent flow structures. Tones appear in the spectra for $M \geq 1.1$ for the untripped jets and $M \geq 0.8$ for the tripped jets, respectively. They are found for the same frequencies and azimuthal modes as the tones in the velocity spectra at $z = 0.4r_0$, showing that the flow structures persist at the feedback frequencies down to the plate. However, the velocity spectra exhibit differences depending on the initial flow conditions. The levels are higher for the initially laminar jets than for the highly-disturbed jets, in agreement with the stronger shear-layer velocity fluctuations in figures 3(c,f). The tones emerge more weakly in the former case than in the latter case, suggesting a weaker resonance for the non-disturbed jets. For $M = 0.8$ and $M = 1.3$ in figures 10(b,f) and (d,h), harmonics of the dominant tone for n_θ are present for the tripped jets but not for the untripped jets, confirming a weaker coupling between the jet flow and the pressure waves for the untripped jets.

F. Power gains of the Kelvin-Helmholtz instability waves between the nozzle and the plate

In this section, the total amplification of the instability waves between the nozzle and the plate is computed to discuss the origin of the variations of the amplitude of the dominant tone with the state of the nozzle-exit mixing layer, as done in recent work [33]. To characterize the development of the instability waves in the jets, an inviscid spatial stability analysis is performed from the hyperbolic-tangent velocity profile [48]:

$$\frac{u_z(r)}{u_j} = \frac{1}{2} \left[1 - \tanh \left(\frac{1}{2} \frac{(r - r_0)}{\delta_\theta(z)} \right) \right] \quad (2)$$

where $\delta_\theta(z)$ is the shear-layer momentum thickness obtained in the LES. The LES mean velocity profiles are not used because they contain strong flow oscillations near the plate, making the linear stability analysis difficult. As in previous investigations [49, 50], the compressible Rayleigh equation is solved with a shooting technique [51], employing the Euler method for the integration step and the secant method for the search of the complex wavenumber. For a given Strouhal number St , the growth rates $-k_i$ of the instability waves, where k_i is the imaginary part of the wavenumber, are first evaluated at $z = 0$ for a hyperbolic-tangent profile of thickness $\delta_\theta(z = 0)$. The growth rates for the other axial

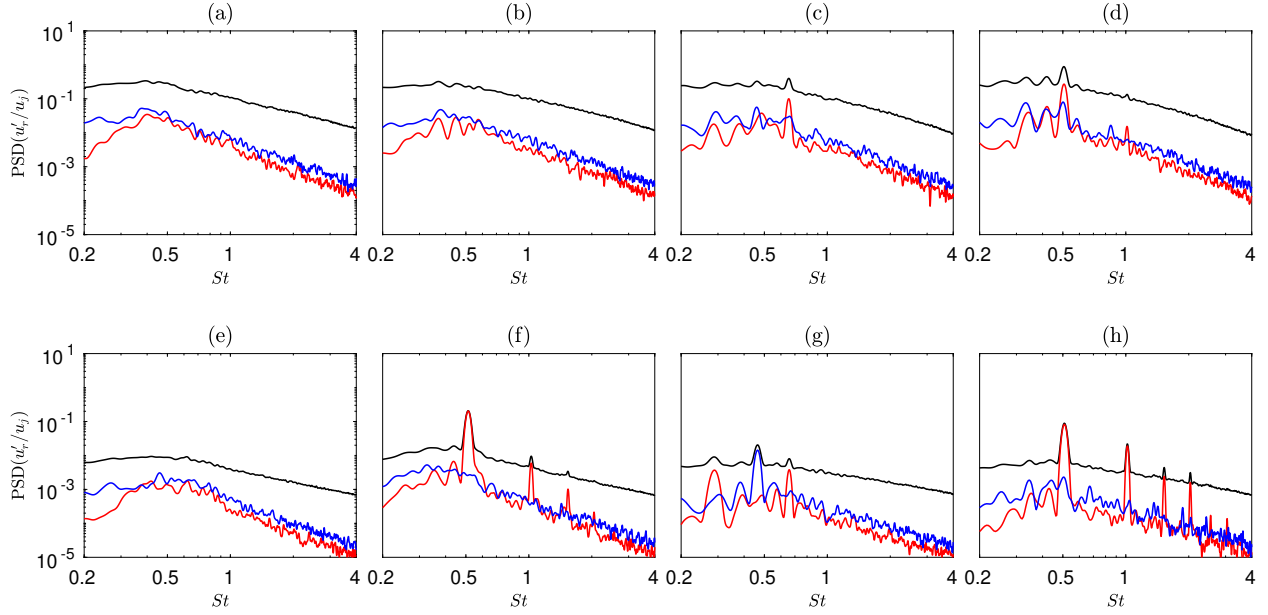


Fig. 10 Power spectral densities of the fluctuations of radial velocity at $r = r_0$ and $z = 7r_0$ for the (top) untripped and (bottom) tripped jets for (a,e) $M = 0.6$, (b,f) $M = 0.8$, (c,g) $M = 1.1$ and (d,h) $M = 1.3$, — full signal, — $n_\theta = 0$ and — $n_\theta = 1$.

locations are deduced from these results using a scaling with the shear-layer thickness $\delta_\theta(z)$ [48]. The wavenumbers of damped waves with $k_i \geq 0$ are not accurately estimated by the solving of the Rayleigh equation [51]. Their imaginary parts are thus set to zero in what follows.

The growth rates normalized by the jet radius r_0 obtained for $n_\theta = 0$ between $z = 0$ and $8r_0$ are presented in figure 11 for the untripped and tripped jets at $M = 0.6, 0.8, 1.1$ and 1.3 . The spatial variations of the growth rates are similar for all jets. Near the nozzle, they are highest for Strouhal numbers higher than 1. The most unstable frequencies decrease with the axial distance due to the shear-layer thickening [50, 52]. They are reduced down to $St = 0.5$ at $z = 2r_0$ and they reach Strouhal numbers lower than 0.2 near the plate. Therefore, the high-frequency instability waves grow over a few radii downstream of the nozzle exit whereas the low-frequency instability waves are amplified all over the nozzle-to-plate distance. For both boundary-layer states, the growth rates decrease as the Mach number increases, indicating that the jet flow is more stable for higher Mach numbers, as expected [48, 51]. However, differences are noticed between the two initial flow conditions. Downstream of the nozzle, the growth rates for $St \geq 0.5$ remain high over a longer distance for the untripped jets than for the tripped jets, typically of $2r_0$ in the first case and r_0 in the second. This can be due to the slower spreading of the mixing layer near the nozzle in the untripped jets, illustrated in figure 3(b,e). On the contrary, for $z \geq 4r_0$ and $St \leq 0.5$, the growth rates are lower for the untripped jets than for the tripped jets, indicating weaker large-scale structures in the former case.

To quantify the amplification of the instability waves between the nozzle and the plate, the growth rates of the Kelvin-Helmholtz waves are integrated between $z = 0$ and L , as done in previous works [30, 33, 53–56], giving the power gain A :

$$A(St) = \exp\left(\int_0^L -k_i(St, z) dz\right) \quad (3)$$

For $n_\theta = 0$, the power gains A_{untrip} and A_{trip} for the untripped and tripped jets, respectively, are computed at the frequency of the tones in the near-nozzle pressure spectra. The values obtained are gathered in table 1, where the highest gain value for each Mach number is shown in bold. For $M = 0.6$, the gain is given at the Strouhal number $St = 0.83$, for which there is a peak for the untripped jet but not for the tripped one. The value of the gain is higher in the first case than in the second case, as expected. For Mach numbers between 0.75 and 1.1, the power gains at the tone frequencies are higher for the initially disturbed jets than for the initially laminar ones. The shear-layer instability waves at the

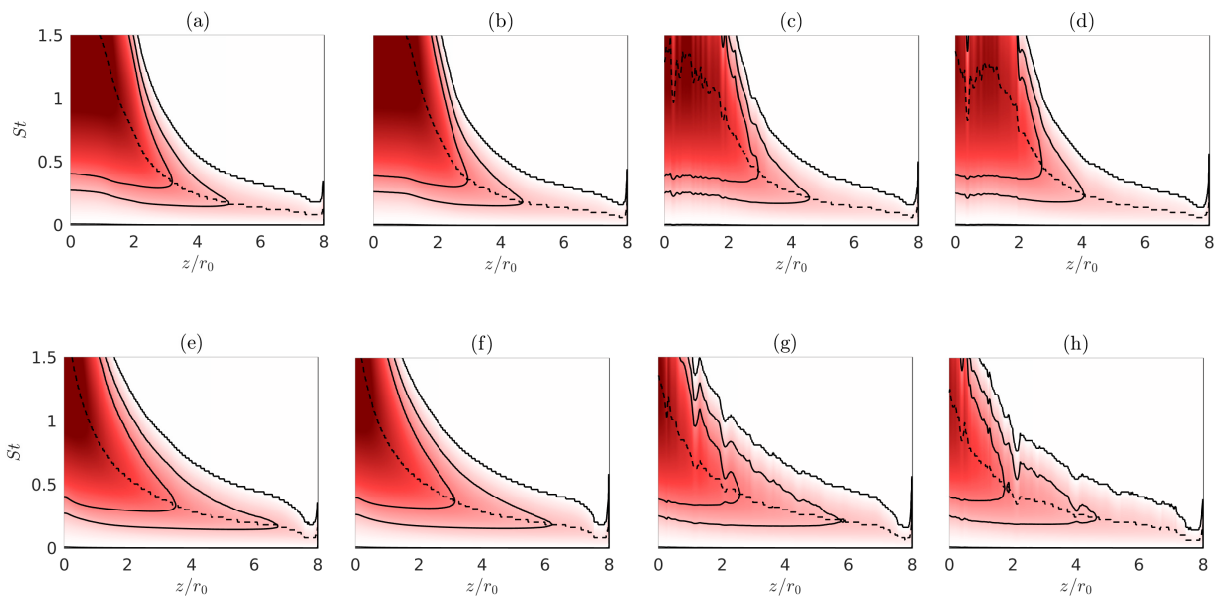


Fig. 11 Instability growth rates $-k_i r_0$ for $n_\theta = 0$ as a function of the axial position z and of the Strouhal number St for the (top) untripped and (bottom) tripped jets and at (a,e) $M = 0.6$, (b,f) $M = 0.8$, (c,g) $M = 1.1$ and (d,h) $M = 1.3$, --- most unstable frequencies. Contour lines for the levels 0, 0.5 and 1 are drawn in black. The colorscale ranges from -3 to 3, from blue to red.

feedback frequencies are thus more amplified between the nozzle and the plate in the first case, which may explain the stronger tones in the near-nozzle pressure spectra. For $M = 1.3$, the power gain at the tone frequency is the highest for the untripped jet. However, the tone in the pressure spectrum of this jet is weaker than that for the tripped jet. This mismatch may be due to uncertainties in the calculation of the gain, in particular the facts that a hyperbolic-tangent velocity profile is used and that the damping of the instability waves is not taken into account.

M	0.6	0.75	0.8	0.9	1	1.1	1.3
St	0.83	0.61	0.51	0.40	0.31	0.29	0.51
$A_{untrip}(St)$	566	180	117	55	39	37	74
$A_{trip}(St)$	212	226	185	104	137	106	37

Table 1 Peak Strouhal numbers St for $n_\theta = 0$ and power gains A_{untrip} and A_{trip} at this frequency of the shear-layer instability waves between the nozzle and the plate for the untripped and tripped jets.

IV. Conclusion

In this paper, the tone generation in impinging jets with laminar and highly-disturbed nozzle-exit boundary layers has been investigated using LES for Mach numbers varying between 0.6 and 1.3. For the initially laminar jets at $M \leq 0.8$ and the highly-disturbed jet at $M = 0.6$, the noise emitted by the jets in the upstream direction is broadband. For higher Mach numbers, intense tones are produced by feedback mechanisms establishing between the nozzle and the plate, consisting of downstream-travelling Kelvin-Helmholtz instability waves and free-stream upstream-travelling guided jet waves. The frequencies of the tones are similar regardless of the initial flow condition. They are located in the bands of the guided jet waves closing the feedback loops, as expected. However, the amplitudes and prominence of the tones are lower for the initially laminar jets than for the highly-disturbed jets, indicating a weaker resonance. In the

same way as for the pressure spectra, tones are present in the shear-layer velocity spectra. They are less prominent for the laminar jets than for the highly-disturbed jets, suggesting a weaker forcing of the jet flow structures by the upstream-propagating pressure waves. This weaker forcing may be related to the presence of vortex pairings in the shear layers of the non-disturbed jets near the most unstable shear-layer frequency. For each Mach number, the amplifications of the shear-layer instability waves between the nozzle and the plate have been computed at the tone frequencies for the two exit boundary-layer states. In most cases, at a given Mach number, the strongest tone is found for the jet for which this amplification is highest, highlighting the role of the growth of the instability waves on the tone generation. Consequently, the boundary-layer state strongly affects the amplitudes of the tones, which may change the dominant feedback mode. The initial flow state has, however, little effects on the tone frequencies. Thus, this work shows that the differences in the tonal frequencies between the present simulations and the experiments of Jaunet *et al.* [32] do not appear to be fully explained by differences in this state. In future works, it would be relevant to investigate the influence of other nozzle-exit conditions on the frequencies of the tones emitted by impinging jets, such as the shear-layer thickness or the shape of the nozzle-exit velocity profiles.

Acknowledgments

This work was financed by ArianeGroup and the DGA (Direction Générale de l'Armement). It was also financially supported by the IRICE IJES project RA0014963 (Installed Jet Effect Simulator, FEDER-FSE Rhône-Alpes). This work was granted access to the HPC resources of PMCS2I (Pôle de Modélisation et de Calcul en Sciences de l'Ingénieur et de l'Information) of Ecole Centrale de Lyon, PSMN (Pôle Scientifique de Modélisation Numérique) of ENS de Lyon and P2CHPD (Pôle de Calcul Hautes Performances Dédiés) of Université Lyon I, members of FLMSN (Fédération Lyonnaise de Modélisation et Sciences Numériques), partner of EQUIPEX EQUIP@MESO, and to the resources of TGCC (Très Grand Centre de calcul du CEA). It was performed within the framework of the Labex CeLyA of Université de Lyon, operated by the French National Research Agency (grant no. ANR-10-LABX-0060/ANR-16-IDEX-0005).

References

- [1] Marsh, A. H., "Noise measurements around a subsonic air jet impinging on a plane, rigid surface," *J. Acoust. Soc. Am.*, Vol. 33, No. 8, 1961, pp. 1065–1066. <https://doi.org/10.1121/1.1908894>.
- [2] Preisser, J. S., "Fluctuating surface pressure and acoustic radiation for subsonic normal jet impingement," *NASA Technical Paper 1361*, 1979.
- [3] Neuwerth, G., "Acoustic feedback of a subsonic and supersonic free jet which impinges on an obstacle," *NASA Technical Translation No. F-15719*, 1974.
- [4] Ho, C.-M., and Nosseir, N. S., "Dynamics of an impinging jet. Part 1. The feedback phenomenon," *J. Fluid Mech.*, Vol. 105, 1981, pp. 119–142. <https://doi.org/10.1017/S0022112081003133>.
- [5] Nosseir, N. S., and Ho, C.-M., "Dynamics of an impinging jet. Part 2. The noise generation," *J. Fluid Mech.*, Vol. 116, 1982, pp. 379–391. <https://doi.org/10.1017/S0022112082000512>.
- [6] Norum, T. D., "Supersonic rectangular jet impingement noise experiments," *AIAA J.*, Vol. 29, No. 7, 1991, pp. 1051–1057. <https://doi.org/10.2514/3.10703>.
- [7] Krothapalli, A., Rajkuperan, E., Alvi, F., and Lourenco, L., "Flow field and noise characteristics of a supersonic impinging jet," *J. Fluid Mech.*, Vol. 392, 1999, pp. 155–181. <https://doi.org/10.1017/S0022112099005406>.
- [8] Henderson, B., and Powell, A., "Experiments concerning tones produced by an axisymmetric choked jet impinging on flat plates," *J. Sound Vib.*, Vol. 168, No. 2, 1993, pp. 307–326. <https://doi.org/10.1006/jsvi.1993.1375>.
- [9] Henderson, B., "The connection between sound production and jet structure of the supersonic impinging jet," *J. Acoust. Soc. Am.*, Vol. 111, No. 2, 2002, pp. 735–747. <https://doi.org/10.1121/1.1436069>.
- [10] Henderson, B., Bridges, J., and Wernet, M., "An experimental study of the oscillatory flow structure of tone-producing supersonic impinging jets," *J. Fluid Mech.*, Vol. 542, 2005, pp. 115–137. <https://doi.org/10.1017/S0022112005006385>.
- [11] Dauplain, A., Gicquel, L., and Moreau, S., "Large-eddy simulation of supersonic impinging jets," *AIAA J.*, Vol. 50, No. 7, 2012, pp. 1560–1574. <https://doi.org/10.2514/1.J051470>.

- [12] Gojon, R., Bogey, C., and Marsden, O., "Investigation of tone generation in ideally expanded supersonic planar impinging jets using large-eddy simulation," *J. Fluid Mech.*, Vol. 808, 2016, pp. 90–115. <https://doi.org/10.1017/jfm.2016.628>.
- [13] Gojon, R., and Bogey, C., "Flow structure oscillations and tone production in underexpanded impinging round jets," *AIAA J.*, Vol. 55, No. 6, 2017, pp. 1792–1805. <https://doi.org/10.2514/1.J055618>.
- [14] Bogey, C., and Gojon, R., "Feedback loop and upwind-propagating waves in ideally expanded supersonic impinging round jets," *J. Fluid Mech.*, Vol. 823, 2017, pp. 562–591. <https://doi.org/10.1017/jfm.2017.334>.
- [15] Powell, A., "On edge tones and associated phenomena," *Acta Acustica United with Acustica*, Vol. 3, No. 4, 1953, pp. 233–243.
- [16] Umeda, Y., Maeda, H., and Ishii, R., "Hole tone generated from almost choked to highly choked jets," *AIAA J.*, Vol. 26, No. 9, 1988, pp. 1036–1043. <https://doi.org/10.2514/3.10009>.
- [17] Umeda, Y., and Ishii, R., "Hole tone generation from highly choked jets," *J. Acoust. Soc. Am.*, Vol. 94, No. 2, 1993, pp. 1058–1066. <https://doi.org/10.1121/1.406952>.
- [18] Varé, M., and Bogey, C., "Generation of acoustic tones in round jets at a Mach number of 0.9 impinging on a plate with and without a hole," *J. Fluid Mech.*, Vol. 936, 2022, p. A16. <https://doi.org/10.1017/jfm.2022.47>.
- [19] Gojon, R., and Bogey, C., "Effects of the angle of impact on the aeroacoustic feedback mechanism in supersonic impinging planar jets," *International Journal of Aeroacoustics*, Vol. 18, No. 2-3, 2019, pp. 258–278. <https://doi.org/10.1177/1475472X18812808>.
- [20] Tam, C., and Ahuja, K., "Theoretical model of discrete tone generation by impinging jets," *J. Fluid Mech.*, Vol. 214, 1990, pp. 67–87. <https://doi.org/10.1017/S0022112090000052>.
- [21] Jordan, P., Jaunet, V., Towne, A., Cavalieri, A., Colonius, T., Schmidt, O., and Agarwal, A., "Jet-flap interaction tones," *J. Fluid Mech.*, Vol. 853, 2018, pp. 333–358. <https://doi.org/10.1017/jfm.2018.566>.
- [22] Tam, C., and Chandramouli, S., "Jet-plate interaction tones relevant to over-the-wing engine mount concept," *J. Sound Vib.*, Vol. 486, 2020, p. 115378. <https://doi.org/10.1016/j.jsv.2020.115378>.
- [23] Gojon, R., Bogey, C., and Mihaescu, M., "Oscillation modes in screeching jets," *AIAA J.*, Vol. 56, No. 7, 2018, pp. 2918–2924. <https://doi.org/10.2514/1.J056936>.
- [24] Edgington-Mitchell, D., Jaunet, V., Jordan, P., Towne, A., Soria, J., and Honnery, D., "Upstream-travelling acoustic jet modes as a closure mechanism for screech," *J. Fluid Mech.*, Vol. 855, 2018. <https://doi.org/10.1017/jfm.2018.642>.
- [25] Gojon, R., Gutmark, E., and Mihaescu, M., "Antisymmetric oscillation modes in rectangular screeching jets," *AIAA J.*, Vol. 57, No. 8, 2019, pp. 3422–3441. <https://doi.org/10.2514/1.J057514>.
- [26] Mancinelli, M., Jaunet, V., Jordan, P., and Towne, A., "Screech-tone prediction using upstream-travelling jet modes," *Experiments in Fluids*, Vol. 60, No. 1, 2019, p. 22. <https://doi.org/10.1007/s00348-018-2673-2>.
- [27] Towne, A., Cavalieri, A. V. G., Jordan, P., Colonius, T., Schmidt, O., Jaunet, V., and Brès, G. A., "Acoustic resonance in the potential core of subsonic jets," *J. Fluid Mech.*, Vol. 825, 2017, pp. 1113–1152. <https://doi.org/10.1017/jfm.2017.346>.
- [28] Schmidt, O. T., Towne, A., Colonius, T., Cavalieri, A. V. G., Jordan, P., and Brès, G. A., "Wavepackets and trapped acoustic modes in a turbulent jet: coherent structure eduction and global stability," *J. Fluid Mech.*, Vol. 825, 2017, pp. 1153–1181. <https://doi.org/10.1017/jfm.2017.407>.
- [29] Bogey, C., "Acoustic tones in the near-nozzle region of jets: characteristics and variations between Mach numbers 0.5 and 2," *J. Fluid Mech.*, Vol. 921, 2021. <https://doi.org/10.1017/jfm.2021.426>.
- [30] Bogey, C., "Interactions between upstream-propagating guided jet waves and shear-layer instability waves near the nozzle of subsonic and nearly ideally expanded supersonic free jets with laminar boundary layers," *J. Fluid Mech.*, Vol. 949, 2022, p. A41. <https://doi.org/10.1017/jfm.2022.776>.
- [31] Wagner, F., *The sound and flow field of an axially symmetric free jet upon impact on a wall*, National Aeronautics and Space Administration, 1971.
- [32] Jaunet, V., Mancinelli, M., Jordan, P., Towne, A., Edgington-Mitchell, D. M., Lehnasch, G., and Girard, S., "Dynamics of round jet impingement," *AIAA Paper 2019-2769*, 2019. <https://doi.org/10.2514/6.2019-2769>.

- [33] Varé, M., and Bogey, C., “Mach number dependence of tone generation by impinging round jets,” *accepted for publication in AIAA J.*, 2023.
- [34] Zaman, K., “Effect of initial condition on subsonic jet noise,” *AIAA J.*, Vol. 23, No. 9, 1985, pp. 1370–1373. <https://doi.org/10.2514/3.9094>.
- [35] Bridges, J., and Hussain, A., “Roles of initial condition and vortex pairing in jet noise,” *J. Sound Vib.*, Vol. 117, No. 2, 1987, pp. 289–311. [https://doi.org/10.1016/0022-460X\(87\)90540-2](https://doi.org/10.1016/0022-460X(87)90540-2).
- [36] Bogey, C., Marsden, O., and Bailly, C., “Influence of initial turbulence level on the flow and sound fields of a subsonic jet at a diameter-based Reynolds number of 10^5 ,” *J. Fluid Mech.*, Vol. 701, 2012, pp. 352–385. <https://doi.org/10.1017/jfm.2012.162>.
- [37] Brès, G., Jordan, P., Jaunet, V., Le Rallic, M., Cavalieri, A., Towne, A., Lele, S., Colonius, T., and Schmidt, O., “Importance of the nozzle-exit boundary-layer state in subsonic turbulent jets,” *J. Fluid Mech.*, Vol. 851, 2018, pp. 83–124. <https://doi.org/10.1017/jfm.2018.476>.
- [38] Bogey, C., Marsden, O., and Bailly, C., “Large-eddy simulation of the flow and acoustic fields of a Reynolds number 10^5 subsonic jet with tripped exit boundary layers,” *Phys. Fluids*, Vol. 23, No. 3, 2011, p. 035104. <https://doi.org/10.1063/1.3555634>.
- [39] Berland, J., Bogey, C., Marsden, O., and Bailly, C., “High-order, low dispersive and low dissipative explicit schemes for multiple-scale and boundary problems,” *J. Comput. Phys.*, Vol. 224, No. 2, 2007, pp. 637–662. <https://doi.org/10.1016/j.jcp.2006.10.017>.
- [40] Bogey, C., and Bailly, C., “A family of low dispersive and low dissipative explicit schemes for flow and noise computations,” *J. Computat. Phys.*, Vol. 194, No. 1, 2004, pp. 194–214. <https://doi.org/10.1016/j.jcp.2003.09.003>.
- [41] Fauconnier, D., Bogey, C., and Dick, E., “On the performance of relaxation filtering for large-eddy simulation,” *J. Turbul.*, Vol. 14, No. 1, 2013, pp. 22–49. <https://doi.org/10.1080/14685248.2012.740567>.
- [42] Bogey, C., De Cacqueray, N., and Bailly, C., “A shock-capturing methodology based on adaptative spatial filtering for high-order non-linear computations,” *J. Comput. Phys.*, Vol. 228, No. 5, 2009, pp. 1447–1465. <https://doi.org/10.1016/j.jcp.2008.10.042>.
- [43] Tam, C., and Dong, Z., “Radiation and outflow boundary conditions for direct computation of acoustic and flow disturbances in a non uniform mean flow,” *J. Comput. Acoust.*, Vol. 4, No. 02, 1996, pp. 175–201. <https://doi.org/10.1142/S0218396X96000040>.
- [44] Bogey, C., and Bailly, C., “Three-dimensional non-reflective boundary conditions for acoustic simulations: far-field formulation and validation test cases,” *Acta Acustica united with Acustica*, Vol. 88, No. 4, 2002, pp. 463–471.
- [45] Mohseni, K., and Colonius, T., “Numerical treatment of polar coordinate singularities,” *J. Comput. Phys.*, Vol. 157, No. 2, 2000, pp. 787–795. <https://doi.org/10.1006/jcph.1999.6382>.
- [46] Bogey, C., De Cacqueray, N., and Bailly, C., “Finite differences for coarse azimuthal discretization and for reduction of effective resolution near origin of cylindrical flow equations,” *J. Comput. Phys.*, Vol. 230, No. 4, 2011, pp. 1134–1146. <https://doi.org/10.1016/j.jcp.2010.10.031>.
- [47] Bogey, C., “Grid sensitivity of flow field and noise of high-Reynolds-number jets computed by large-eddy simulation,” *International Journal of Aeroacoustics*, Vol. 17, No. 4-5, 2018, pp. 399–424. <https://doi.org/10.1177/1475472X18778287>.
- [48] Michalke, A., “Survey on jet instability theory,” *Progress in Aerospace Sciences*, Vol. 21, 1984, pp. 159–199. [https://doi.org/10.1016/0376-0421\(84\)90005-8](https://doi.org/10.1016/0376-0421(84)90005-8).
- [49] Bogey, C., and Sabatini, R., “Effects of nozzle-exit boundary-layer profile on the initial shear-layer instability, flow field and noise of subsonic jets,” *J. Fluid Mech.*, Vol. 876, 2019, pp. 288–325. <https://doi.org/10.1017/jfm.2019.546>.
- [50] Bogey, C., “Generation of excess noise by jets with highly disturbed laminar boundary-layer profiles,” *AIAA J.*, Vol. 59, No. 2, 2021, pp. 569–579. <https://doi.org/10.2514/1.J059610>.
- [51] Morris, P., “The instability of high speed jets,” *International Journal of Aeroacoustics*, Vol. 9, No. 1-2, 2010, pp. 1–50. <https://doi.org/10.1260/1475-472X.9.1-2.1>.
- [52] Karami, S., Edgington-Mitchell, D., Theofilis, V., and Soria, J., “Characteristics of acoustic and hydrodynamic waves in under-expanded supersonic impinging jets,” *J. Fluid Mech.*, Vol. 905, 2020. <https://doi.org/10.1017/jfm.2020.740>.
- [53] Woolley, J., and Karamcheti, K., “The role of jet stability in edgetone generation,” *AIAA Paper*, , No. 73-628, 1973, pp. 1–35. <https://doi.org/10.2514/6.1973-628>.

- [54] Woolley, J., and Karamcheti, K., "Role of jet stability in edgetone generation," *AIAA J.*, Vol. 12, No. 11, 1974, pp. 1457–1458. <https://doi.org/10.2514/3.49525>.
- [55] Tam, C., Chen, P., and Seiner, J., "Relationship between the instability waves and noise of high-speed jets," *AIAA J.*, Vol. 30, No. 7, 1992, pp. 1747–1752. <https://doi.org/10.2514/3.11132>.
- [56] Muller, F., Vuillot, F., Rahier, G., and Casalis, G., "Modal analysis of a subsonic hot jet LES with comparison to the linear stability analysis," *AIAA Paper*, 2005, p. 2886. <https://doi.org/10.2514/6.2005-2886>.